Book ISBN: 978-952-412-288-7 | Series ISSN 2709-7609 (Online) | License: CC BY-NC-ND 4.0 | Pages: 10

INVESTIGATION OF SIMILARITY PARAMETERS IN ISENTROPIC SUPERSONIC EXPANSIONS OF ORGANIC VAPORS

Marta Zocca[1*], Marta Pederzolli[2,1], Teemu Turunen-Saaresti[1], Alberto Guardone[2,1]

[1] *Laboratory of Fluid Dynamics, School of Energy Systems, LUT University, Yliopistonkatu 34, 53850 Lappeenranta, Finland*

[2] *Department of Aerospace Science & Technology, Politecnico di Milano, Via La Masa 34, 20156 Milan, Italy*

* Corresponding Author: marta.zocca@lut.fi

ABSTRACT

This paper presents a theoretical investigation into similarity parameters in supersonic expansions of organic vapors like the ones encountered in supersonic turbines for Organic Rankine Cycle (ORC) applications. Building on previous studies of one-dimensional isentropic expansions in the single-phase region of organic fluids near the vapor-liquid saturation curve and critical point, this research investigates more on the behavior of the compressibility factor along isentropic expansions, as the value of the compressibility factor seems to represent an adequate similarity parameter based on experimental data, although several elements from the theory of non-ideal compressible fluid flows might suggest otherwise. Using a Helmholtz energy-based Span-Wagner Equation of State, the study examines a one-dimensional model for isentropic expansions to identify suitable similarity parameters characterizing such flows in non-ideal conditions. The compressibility factor in total conditions Z^{t} is confirmed as a key similarity parameter, correlating with similar trends in several relevant variables for experimentation. This parameter may simplify the preliminary design of thermodynamic cycles and components, reduce design variables, streamline testing in pilot plants, and facilitate the preparation of performance and operating maps, offering time and cost savings. The findings of this work are particularly relevant for ORC turbines, where expansions typically occur under moderately high non-ideal conditions ($Z^{\mathrm{t}} > 0.5$).

1. INTRODUCTION

Supersonic expansions of organic vapors are encountered in several technical applications, including rocket propulsion, oil and gas applications, heat pumps, refrigeration, and pharmaceutical production. In Organic Rankine Cycle (ORC) applications (see e.g. Colonna *et al.* (2015)), supersonic expansions of organic vapors are relevant especially in connection with turbine expansions, which occur in thermodynamic conditions where the molecularly complex organic compounds used as working fluid in the power cycles undergo transformations that cannot be adequately described by textbook gas dynamics of dilute, ideal gases. Non-Ideal Compressible Fluid Dynamics (NICFD) is the branch of gasdynamics that studies flows typical of ORC applications, namely flows of fluids in thermodynamic and chemical equilibrium, under conditions where the compressibility factor $Z = Pv/RT \neq 1$. In ideal-gas conditions, $Pv = RT$, and $Z = 1$, where P is pressure, v is mass specific volume, R is the gas constant, and T is temperature. Nonideal gasdynamic effects in single-phase flows are notable near the liquid-vapor saturation curve, at the critical point, or under supercritical conditions (see e.g. Guardone *et al.* (2024)).

Testing such flows in experimental facilities presents significant challenges, as conventional measurement techniques need to be adapted to handle the elevated pressure and temperature levels required for studying NICFD effects and to tackle condensation issues. Systematic experimental investigation of

NICFD flows have become reality only relatively recently, as reviewed by Spinelli *et al.* (2020) and aus der Wiesche (2023). The continuous need for detailed measurements to characterize NICFD flows motivates the need to establish the right set of similarity parameters for designing components and flow devices subjected to non-ideal compressible flows.

The purpose of this work is to continue the investigation on similarity parameters in isentropic supersonic expansions of organic vapors, building on recent contributions from different groups in the ORC community, particularly the work of Conti *et al.* (2021) and aus der Wiesche and Reinker (2022). Conti *et al.* (2021) concluded that the compressibility factor in total conditions Z^{t} is a suitable similarity parameter for characterizing isentropic expansions of complex fluids in moderately high non-ideal conditions. aus der Wiesche and Reinker (2022) emphasized the importance of considering the constant-entropy gradients of the compressibility factor Z in the list of similarity parameters for turbomachinery flows. In their work, aus der Wiesche and Reinker (2022) stressed the need for at least one similarity number specifically addressing flow non-ideality when developing scaling laws for organic vapor turbomachinery. They proposed a modified Eckert number, Ec^{*}, with a generalized formulation for non-ideal flows, and introduced the Traupel number, Tr, which incorporates the isentropic derivative of the compressibility factor, $(\partial Z/\partial P)_s$. The present study does not yet aim to develop scaling laws for turbomachinery, but instead focuses on the one-dimensional modeling required to design wind tunnel testing of static components such as de Laval nozzles, and on the generation of uniform flow conditions in wind tunnel experiments, particularly for probe calibration purposes. Despite the limitations noted by aus der Wiesche and Reinker (2022), using Z^{t} as a similarity parameter remains advantageous, especially in experimental contexts, due to its practical simplicity. Once pressure and temperature are known or measured, a single evaluation of the equation of state is sufficient to determine the fluid density, making Z^{t} readily accessible even during experimental runs. Moreover, within the conceptual framework of the principle of corresponding states, the compressibility factor displays a universal character if fluids are compared using reduced variables. Although the principle of corresponding states does not apply to non-ideal compressible fluid dynamics if more complex equations of state than the van der Waals model are adopted, the idea of comparing fluid properties in reduced variables is conceptually familiar and convenient.

The paper is structured as follows: Section 2 reviews the theoretical background and presents the methodology adopted in this study. Section 3 presents and discusses the results concerning isentropic expansions. Conclusions are drawn in Section 4.

2. THEORETICAL BACKGROUND AND METHODOLOGY

2.1 Perfect vapors and non-ideal vapors

In the study of NICFD, flow regimes are typically classified based on the value of the thermodynamic variable $\Gamma = 1 + (\rho/c)(\partial c/\partial \rho)_s$, known as the fundamental derivative of gasdynamics, where ρ is density, c is speed of sound, and s is entropy. Ideal-like behavior of flows is observed for $\Gamma > 1$, indicating that the speed of sound increases with pressure, which is typical for most substances. For instance, in a polytropic ideal gas, the fundamental derivative Γ simplifies to $\Gamma = (\gamma + 1)/2$, which is always positive and greater than 1 as the specific heat ratio γ is always > 1. For $0 < \Gamma < 1$, the speed of sound decreases with pressure. In ORC applications, turbine expansions predominantly occur in the so-called non-ideal classical regime ($0 < \Gamma < 1$) in subcritical cycles. In transcritical cycles, the expansion may begin in a region with $\Gamma > 1$ and end in the non-ideal region with $\Gamma < 1$.

Another classification which is particularly relevant for turbomachinery applications is the one proposed by Traupel (1952), which distinguishes between perfect gases, perfect vapors, and non-perfect gases. Perfect gases follow the ideal gas law, while perfect vapors exhibit a unique relationship between compressibility factor and entropy, such that $Z = f(s)$ (aus der Wiesche and Reinker, 2022; Traupel, 1952). Non-perfect gases do not conform to these simplified models and require a more complex analysis based on NICFD theory. Most of the working fluids commonly used in experimental research and industrial

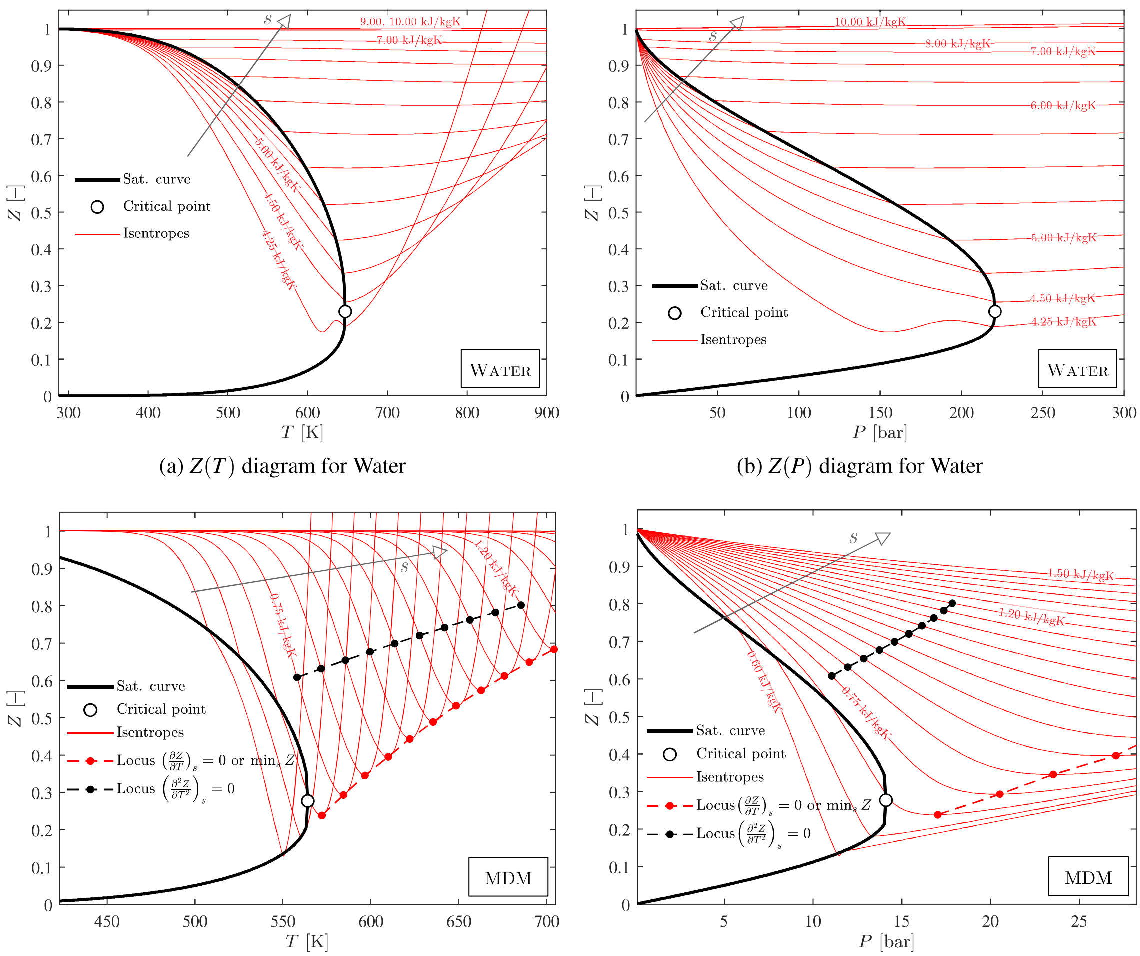

(a) $Z(T)$ diagram for Water

(b) $Z(P)$ diagram for Water

(c) $Z(T)$ diagram for MDM

(d) $Z(P)$ diagram for MDM

Figure 1: $Z(T)$ (a, c) and $Z(P)$ (b, d) diagrams for water (a, b), a perfect vapor, and MDM (c, d), a non-ideal vapor. The red curves represents isentropes in all graphs.

ORC applications fall into this latter category of non-ideal vapors. This study focuses on such fluids, including siloxanes (MDM, MM, D6), halocarbons (R134a, R245fa, R1233zd(E)), alkanes (n-pentane, cyclopentane), and the fluoroketone NOVEC649.

Figure 1 presents the $Z(T)$ and $Z(P)$ diagrams for two substances: steam, a perfect vapor (Figures 1a and 1b), and MDM, a non-ideal vapor (Figures 1c and 1d). These diagrams were generated using a Helmholtz energy-based fundamental relation of the Span-Wagner type, implemented via the CoolProp thermodynamic library (Bell *et al.* (2014)), which is used throughout this work. The diagrams illustrate the compressibility factor as a function of temperature and pressure, expressed in dimensional units of Kelvin and bar, respectively. The diagrams show the compressibility factor at saturation, at the critical point, and along selected isentropes (red curves) ranging from values slightly entering the two-phase region to highly superheated states. Entropy increases in the direction indicated by the arrows, and selected entropy values are labeled along the isentropes in units of kJ/kgK. The profiles of the isentropes in the $Z(T)$ and $Z(P)$ diagrams illustrate the functional dependence of Z on entropy and reveal deviations from perfect-vapor behavior. As expected, and consistent with the early work of Traupel (1952), steam behaves as a perfect vapor over a wide range of application-relevant operating conditions, with Z depending solely on the entropy value (see Figures 1a and 1b). In contrast, for MDM, a molecularly complex organic vapor, the condition $Z = f(s)$ no longer holds. However, some qualitative patterns can be observed in the functional dependence of Z on T and P along isentropes. In Figure 1c, for all superheated entropy levels, the $Z(T)$ curves display a minimum. These minima, corresponding to each plotted isentrope, are marked with red dots. The locus connecting these minima across different entropy levels is indicated by a red dashed line. Along this locus, the gradient $(\partial Z/\partial T)_s$ locally vanishes. Additionally, the $Z(T)$ curves at superheated entropy levels exhibit inflection points, where the second derivative $(\partial^2 Z/\partial T^2)_s = 0$, which are marked with black dots. The locus of these inflection points is traced by a black dashed line. Along each isentrope, the value of Z approaches 1 at increasing temperatures as entropy increases, corresponding to low-pressure levels, consistent with the expected behavior in the dilute-gas region. Figure 1d shows the $Z(P)$ curves at fixed entropy for the same entropy levels considered in Figure 1c. The compressibility factor depends approximately linearly on pressure over an extended region, including superheated and supercritical states, indicating that the gradient $(\partial Z/\partial P)_s$ is approximately constant along isentropes for a wide range of (P,s) relevant to ORC applications. The $Z(P)$ curves gradually deviate from their linear behavior at higher pressures, displaying minima that correspond to those observed in the $Z(T)$ diagram. The locus of these minima is represented in red, corresponding to the locus of $(\partial Z/\partial T)_s = 0$. The locus of $(\partial^2 Z/\partial T^2)_s = 0$ is also shown in black on the $Z(P)$ diagram. Qualitative inspection suggests that this locus is suitable for distinguishing regions where Z behaves approximately linearly with P from regions where this linear behavior fades. As $(\partial^2 Z/\partial P^2)_s$ remains close to zero and changes sign non-systematically, it is challenging to characterize the behavior of the $Z(P)$ curves using quantitative indicators based on the derivatives of Z with respect to pressure. Instead, it is more straightforward to determine the pressure values corresponding to the loci $(\partial Z/\partial T)_s = 0$ and $(\partial^2 Z/\partial T^2)_s = 0$ highlighted in the $Z(T)$ diagram. Similar qualitative distributions of $Z(T)$ and $Z(P)$ at fixed entropy were observed for all the fluids with non-ideal vapor behavior examined in this study, although only the results for MDM are shown in Figure 1 for brevity.

2.2 Boundary conditions and thermodynamic zoning for similarity analysis

The methodology for studying isentropic expansions closely follows that adopted by Conti *et al.* (2021). One-dimensional isentropic expansions are calculated for several total conditions sharing the same total compressibility factor Z^{t}. For each case, the static-to-total property ratios P/P^{t}, ρ/ρ^{t}, T/T^{t}, and c/c^{t} are evaluated over a Mach number range from 0 to 2. These expansions are determined independently of any specific geometric configuration, ensuring generality in the analysis. The calculations are carried out for different levels of non-ideality (Z^{t} between 0.4 and 0.9) and for several pure fluids from different families currently applied in experimental research and industrial ORC applications.

The maximum considered pressure is $2P_c$, and maximum considered temperature is $1.2T_c$. As this study aims to isolate and evaluate the role of Z^{t} as a single similarity parameter in single-phase isentropic expansions, it is important to note that expansions leading to two-phase states are excluded from the analysis. Including two-phase flows would require additional parameters to capture phase-change dynamics, which falls outside the scope of this work. Furthermore, it is recognized that for some fluids, the temperatures considered in this study are above the thermal stability limit of the molecules. However, considering an extended *P*-*T* range allowed here to properly highlight the distribution of Z and Γ on the *P*-*T* thermodynamic plane and to define different zones where the similarity based on the total compressibility factor is studied.

Figure 2 presents the *P*-*T* thermodynamic plane for MDM with P and T expressed in dimensional units. The diagram reports isentropes (red curves), which provide isentropic expansion paths, highlighting their layout over thermodynamic plane. Entropy increases in the direction indicated by the arrow. Black isolines and labels represent the compressibility factor Z. Based on the distribution of the compressibility factor, two loci defined by thick black and thick red dashed curves are retrieved: the former locus represents points where $(\partial^2 Z/\partial T^2)_s = 0$, while latter represents points where the minimum compressibility factor Z along each isentrope occurs ($(\partial Z/\partial T)_s = 0$). Green contours and labels represent the distribution of the fundamental derivative of gasdynamics Γ. The region at $\Gamma < 1$ highlighted on the graph represents the non-ideal region. From the distribution of Γ, two loci are constructed: the locus of minimum Γ along each isentrope (thick blue curve), and the upper, high-pressure branch of the iso-

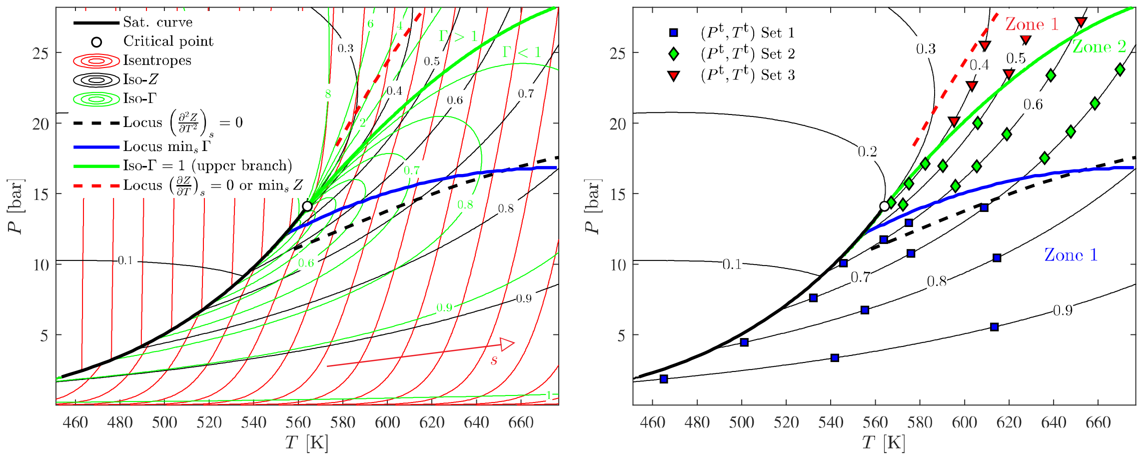

(a) (b)

Figure 2: *P*-*T* diagram of MDM with (a) contours of relevant properties and (b) sets of total conditions $(P^{\mathrm{t}}, T^{\mathrm{t}})$ considered in the similarity study

line $\Gamma = 1$. The four loci represented in Figure 2 subdivide the *P*-*T* plane into distinct regions where volumetric and caloric behavior display different patterns. In summary:

1. The first zone (Zone 1) is the non-ideal region having $0 < \Gamma < 1$, included in the lower-pressure *P*-*T* range in the single-phase region. In this region, the isolines of Γ and Z have the same behavior. Moreover, the speed of sound increases along the expansion for all states, as Γ is everywhere < 1, at least up to the point where the expansion crosses the lower, low-pressure branch of the $\Gamma = 1$ isoline.

2. The second zone (Zone 2) is enclosed between the loci of minimum Γ along isentropes (blue thick curve) and $\Gamma = 1$ (thick green curve). In this region, while the behavior of the speed of sound is expected to be non-ideal as $\Gamma < 1$, the caloric behaviour of the fluid is expected to have a greater influence on the flow dynamics as compared to the first zone, as in this region the iso-Z and iso-Γ have different shapes.

3. The third zone (Zone 3) is enclosed between the isoline $\Gamma = 1$ and the locus of minimum Z along isentropes. The flow displays ideal variation of the speed of sound along the expansion, at least for those states along the expansion that remain enclosed in that region.

The sets of total conditions chosen for the similarity analysis for MDM are displayed in Figure 2b. Three distinct sets are identified: Set 1 corresponds to $(P^{\mathrm{t}}, T^{\mathrm{t}})$ conditions located in Zone 1, Set 2 in Zone 2, and Set 3 in Zone 3. The labels on the black contours represent the values of Z. Conditions corresponding to the same numerical value of Z^{t} but belonging to different regions are chosen, allowing for a comparison of the evolution of flow variables along isentropic expansion for the same value of the compressibility factor in total conditions.

3. SIMILARITY RESULTS

This section presents similarity results obtained for isentropic expansions, beginning with a detailed qualitative investigation using siloxane MDM. While this initial analysis focuses on MDM for clarity and brevity, subsequent quantitative results are reported for one representative fluid from each class considered. These results support broader conclusions on the applicability of the Z^{t}-similarity across different fluid families.

Figure 3 shows the evolution of selected static-to-total property ratios P/P^{t}, ρ/ρ^{t}, T/T^{t}, c/c^{t} (y axes)

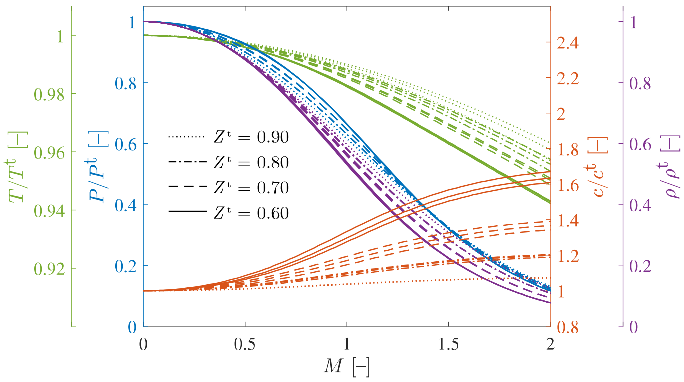

(a) Expansions from $(P^{\mathrm{t}}, T^{\mathrm{t}})$ of Set 1

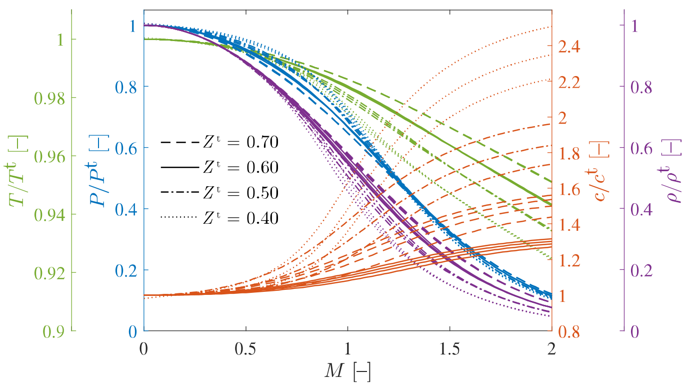

(b) Expansions from $(P^{\mathrm{t}}, T^{\mathrm{t}})$ of Set 2

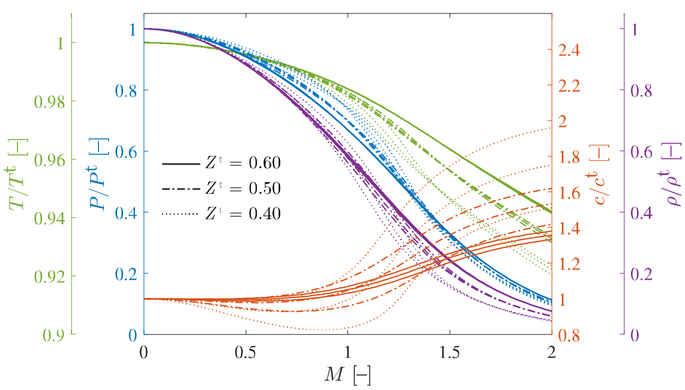

(c) Expansions from $(P^{\mathrm{t}}, T^{\mathrm{t}})$ of Set 3

Figure 3: Static-to-total property ratios along isentropic expansions of MDM starting from the total conditions highlighted in the *P*-*T* diagram of Figure 2b, for Z^{t} equal to 0.4, 0.5, 0.6, 0.7, 0.8, 0.9: (a) Set 1, (b) Set 2, (c) Set 3

along isentropic expansions up to Mach 2 (x axis) obtained from the total conditions represented in Figure 2b, which are grouped into Set 1 (Figure 3a), Set 2 (Figure 3b), and Set 3 (Figure 3c). Each property ratio is represented on a separate y axis and is assigned a different color and a different axis scale. The axis scales for the same property ratios are kept the same across the different plots (Figures 3a, 3b, 3c). The line type on the plot represents the value of Z^{t} for the reported expansion. As expected, the property ratios vary with varying Z^{t} in all studied conditions. This is a well-known non-ideal effect. In Figure 3a, which refers to $(P^{\mathrm{t}}, T^{\mathrm{t}})$ of Set 1 and therefore to the lower-pressure region of the *P*-*T* plane, the $P/P^{\mathrm{t}}(M)$ curves obtained for the same values of Z^{t} (here, 0.6, 0.7, 0.8, and 0.9) almost

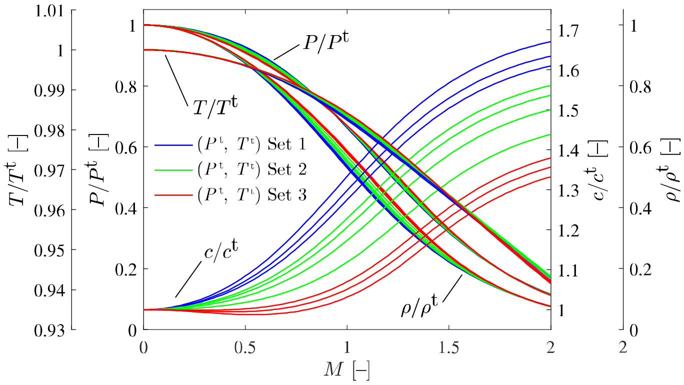

Figure 4: Static-to-total property ratios along isentropic expansions of MDM starting from the total conditions corresponding to $Z^{\mathrm{t}} = 0.6$, but originating from Set 1 (blue), Set 2 (green), Set 3 (red)

perfectly overlap for all Z^{t} and for all states along the expansion, from total conditions to Mach 2. The density ratio and the temperature ratio also display a clear correlation with the value of Z^{t}, although not with the same accuracy as for the pressure ratio. Differences in property ratios at varying Z^{t} are clearly observed on the speed of sound ratio, which, as expected, is the flow property that is mostly influenced by the caloric behavior of the fluid and therefore less suitable for being described by Z^{t} (accounting instead for volumetric behavior) as a similarity parameter. Although the curves obtained at the same value of Z^{t} are observed to cluster close to each other, and separate patterns are observed for each value of Z^{t}, it is clear that the speed of sound ratio cannot be characterized by Z^{t} as a similarity parameter, even in this first region, where the iso-Z and iso-Γ in the P-T plane share a similar layout. Moreover, as expected, the speed of sound increases throughout the expansion for all expansions reported in Figure 3a. Notably, and counter-intuitively, the temperature ratio obtained at the lowest Z^{t} are the ones which exhibit the closest overlap for expansions obtained at the same Z^{t}, with the $Z^{\mathrm{t}} = 0.9$ profiles showing the largest deviations.
Similar considerations apply to the property ratios displayed in Figure 3b, here shown for total conditions $(P^{\mathrm{t}}, T^{\mathrm{t}})$ of Set 2 and for Z^{t} equal to 0.4, 0.5, 0.6, and 0.7. Here, deviations between the density ratios and speed of sound ratios obtained for the same Z^{t} are further amplified compared to the first zone (Figure 3b), and the close overlap of pressure ratios previously observed in Figure 3b is progressively lost for $Z^{\mathrm{t}} > 0.6$, although it maintains below the uncertainty levels of possible static pressure measurements until $Z^{\mathrm{t}} \approx 0.50$. Notably, though, the temperature ratios which in Figure 3a were displaying poor overlap at the same Z^{t} are now more closely superposed. The largest deviations in the T/T^{t} profiles are observed for $Z^{\mathrm{t}} \leq 0.50$ and up to the lower-supersonic branch of the expansion, while the other T/T^{t} profiles display a close overlap at varying Z^{t} otherwise.
For the expansions obtained from the total conditions $(P^{\mathrm{t}}, T^{\mathrm{t}})$ of Set 3, reported in Figure 3c, the same consideration about the clustering of property ratios based on the values of Z^{t} apply, although their overlap gets worse for $Z^{\mathrm{t}} \geq 0.5$. Once more, the pressure ratio has the closest overlap, which is excellent for $Z^{\mathrm{t}} = 0.60$ and degrading for lower Z^{t}.

In Figure 4, the static-to-total property ratios P/P^{t}, ρ/ρ^{t}, T/T^{t}, c/c^{t} are displayed for $Z^{\mathrm{t}} = 0.6$ and for all studied sets of total conditions $(P^{\mathrm{t}}, T^{\mathrm{t}})$. Each y axis reports the scale and range of the corresponding property ratio, while the colors identify the set of total conditions, using the same color convention as in Figure 2b. From Figure 4, the clustering between the property ratios resulting from each set of total conditions is apparent. Therefore, expansions that originate from different zones of the thermodynamic plane but share the same value of Z^{t} display a different behaviour, although a common pattern within each region is clearly identifyable.

Figure 5 shows the sonic-to-total property ratios P^*/P^{t} (Figure 5a) and $(\rho^* c^*)/(\rho^{\mathrm{t}} c^{\mathrm{t}})$ (Figure 5b) as a function of Z^{t} (the x axis) for all studied sets of total conditions $(P^{\mathrm{t}}, T^{\mathrm{t}})$. Results confirm the trends

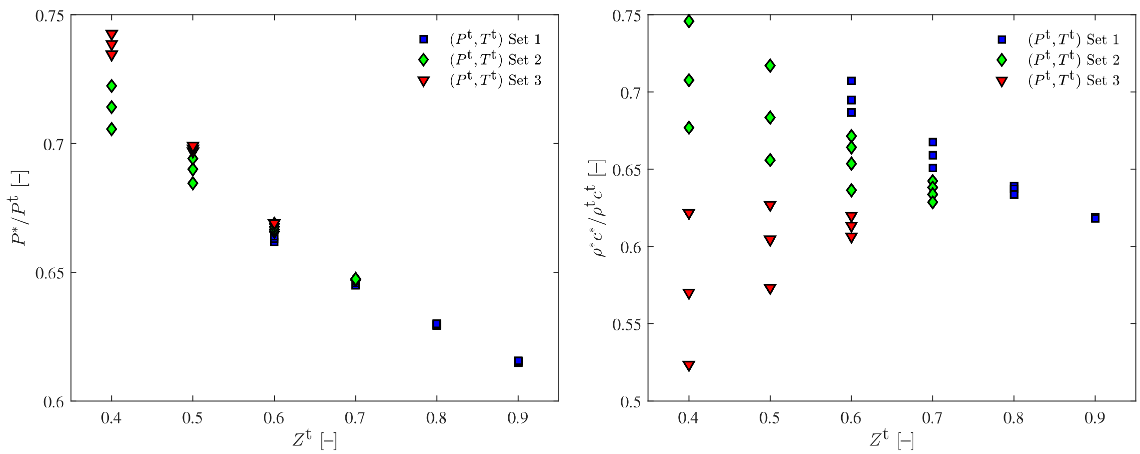

(a) (b)

Figure 5: Critical property ratios (P^*/P^t, a and $\rho^* c^*/\rho^t c^t$, b) along isentropic expansions of MDM starting from the total conditions highlighted in the *P*-*T* diagram of Figure 2b, for Z^t equal to 0.4, 0.5, 0.6, 0.7, 0.8, 0.9: Set 1 (blue square), Set 2 (green diamond), Set 3 (red triangle)

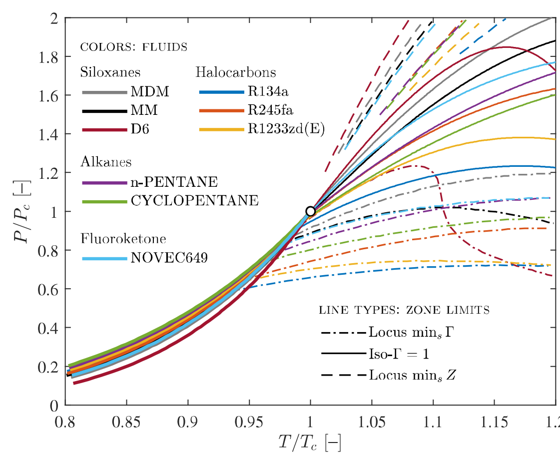

Figure 6: *P*-*T* diagram of all considered fluids in reduced variables. The Mininum-Γ, $\Gamma = 1$, and Minimum-*Z* loci are reported for all fluids.

observed in Figures 3 and 4. While using Z^t as a similarity parameter to determine the sonic momentum density, and therefore the mass flow rate in choked condition is acceptable only for values of Z^t close to ideal conditions and in the first zone below the minimum-Γ locus, the use of Z^t as a similarity parameter to determine the critical pressure ratio is acceptable up to $Z^t = 0.6$ for states below the $\Gamma = 1$ isoline, while satisfactory similarity extends to $Z^t = 0.5$ in the third zone between $\Gamma = 1$ and the minimum-*Z* locus.

Quantitative results are now presented following the qualitative analysis conducted for siloxane MDM. In addition to siloxane MDM, one representative fluid from each class is considered: R1233zd(E) for halocarbons, Cyclopentane for alkanes, and fluoroketone NOVEC649. These fluids exhibit qualitative trends similar to those observed for MDM. The subdivision of the *P*–*T* thermodynamic plane into three zones, as introduced for MDM, is extended to all fluids and shown in Figure 6. The axes are expressed in reduced variables, and the loci used to define the zones are plotted for each fluid. Line styles distinguish the different loci, while colors differentiate the fluids. Consistent with the nomenclature introduced in Section 2.2, the regions bounded by these loci are referred to as Zone 1, Zone 2, and Zone 3 across all

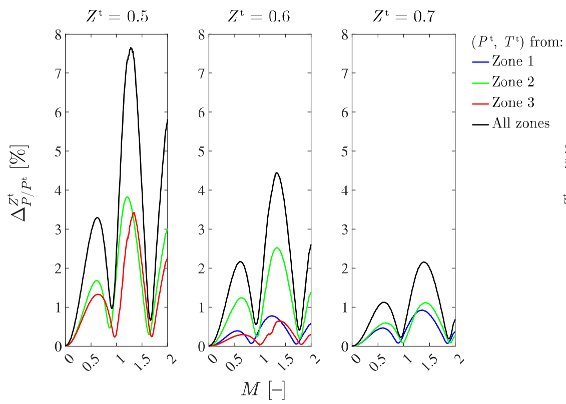

(a) MDM

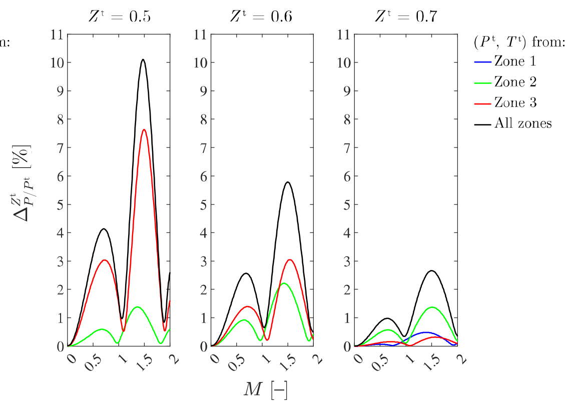

(b) R1233zd(E)

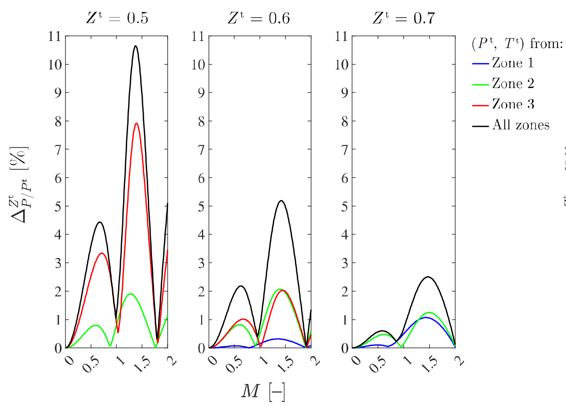

(c) Cyclopentane

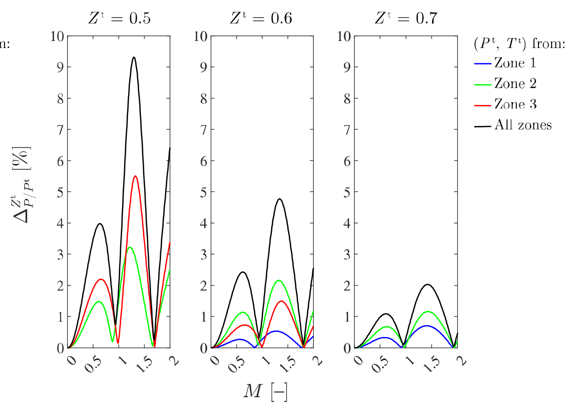

(d) NOVEC649

Figure 7: Spread in pressure ratio values at varying Mach number for expansions characterized by the same Z^t but different (P^t, T^t). Results are reported for four representative fluids.

fluids. Following the methodology of Conti *et al.* (2021), the performance of the total compressibility factor Z^t as a similarity parameter is quantified using the percentage spread in pressure ratio at a given Mach number:

$$\Delta^{Z^t}_{P/P^t} = \frac{\max[P/P^t(Z^t)] - \min[P/P^t(Z^t)]}{\min[P/P^t(Z^t)]} \cdot 100 \tag{1}$$

Here, $\max[P/P^t(Z^t)]$ and $\min[P/P^t(Z^t)]$ represent the maximum and minimum values of the pressure ratio at a given Mach number among all expansions sharing the same Z^t but differing in (P^t, T^t). This metric captures the variation in pressure ratio due to different (P^t, T^t), and is used exclusively since the qualitative analysis already indicated that pressure ratio is the parameter with the best adherence to Z^t-similarity. The spread is evaluated for the four selected fluids, each at three values of Z^t (0.5, 0.6, and 0.7). For each Z^t, total conditions (P^t, T^t) are grouped according to the thermodynamic zone (Zone 1, 2, or 3) they belong to. For comparison, the spread is also computed without distinguishing between zones, i.e., by grouping all conditions with the same Z^t regardless of their thermodynamic region. This allows assessment of Z^t as a similarity parameter both in terms of its absolute value only and in conjunction with thermodynamic zoning.

Figure 7 presents the resulting percentage spreads $\Delta^{Z^t}_{P/P^t}$ as a function of Mach number for each fluid: MDM (Figure 7a), R1233zd(E) (Figure 7b), cyclopentane (Figure 7c), and NOVEC649 (Figure 7d). These trends are consistent across fluids and values of Z^t: (1) the spread across all zones is significantly larger than the spread within individual zones, (2) the spread decreases with increasing Z^t, indicating improved similarity as the fluid behavior approaches ideal-like conditions, and (3) the spread strongly depends on the Mach number, and the trend is similar across all studied fluids and conditions. As anticipated from the qualitative analysis, Zones 2 and 3 tend to produce the highest spreads in pressure ratio, reflecting the stronger influence of caloric effects on flow dynamics in these regions. Notably, though, even under significantly non-ideal conditions, the maximum spread remains below 1% in most expansions originating from Zone 1.

4. CONCLUSIONS

The total compressibility factor, Z^{t}, can serve as a valuable similarity parameter for analyzing non-ideal compressible flows, though its application requires caution. The analysis revealed that similarity based on Z^{t} alone does not hold uniformly across all flow variables or thermodynamic conditions. It is noteworthy that Z^{t}-similarity works well for pressure ratios, which are among the easiest properties to determine from experiments. The findings indicate that Z^{t} alone is not sufficient to ensure similarity across different flow conditions. Instead, both the value of Z^{t} and the thermodynamic region from which the expansion originates play a critical role. This highlights the need for similarity rules that are not only physically meaningful but also practical for experimental application. By identifying representative conditions based on Z^{t} and thermodynamic zoning, it becomes possible to reduce the number of required test cases, thereby streamlining experimental campaigns, such as wind tunnel calibrations, yielding significant time and cost savings. However, caution must be exercised, and additional parameters may be necessary to fully capture the complex, non-ideal behavior of organic vapor flows in ORC applications. Future research should focus on extending the present framework to transcritical cycles and incorporating two-phase expansions to align it with the evolving state of the art in ORC technology.

REFERENCES

aus der Wiesche, S. (2023). Experimental Investigation Techniques for Non-Ideal Compressible Fluid Dynamics. *International Journal of Turbomachinery, Propulsion and Power*, 8(2):11.

aus der Wiesche, S. and Reinker, F. (2022). Dimensional analysis and performance laws for organic vapor flow turbomachinery. *Energy*, 257:124635.

Bell, I. H., Wronski, J., Quoilin, S., and Lemort, V. (2014). Pure and pseudo-pure fluid thermophysical property evaluation and the open-source thermophysical property library CoolProp. *Ind. Eng. Chem. Res.*, 53(6):2498–2508.

Colonna, P., Casati, E., Trapp, C., Mathijssen, T., Larjola, J., Turunen-Saaresti, T., and Uusitalo, A. (2015). Organic Rankine cycle power systems: from the concept to current technology, applications, and an outlook to the future. *J. Eng. Gas Turb. Power*, 137(10):100801. 19 pages.

Conti, C. C., Spinelli, A., and Guardone, A. (2021). Similarity parameters for non-ideal one-dimensional isentropic expansions. In Pini, M. and et al., editors, *Proceedings of NICFD 2020*, volume 28 of *ERCOFTAC Series*, pages 26–35. Springer.

Guardone, A., Colonna, P., Pini, M., and Spinelli, A. (2024). Nonideal compressible fluid dynamics of dense vapors and supercritical fluids. *Annu. Rev. Fluid Mech.*, 56:241–269.

Spinelli, A., Guardone, A., Servi, C. D., Colonna, P., Reinker, F., aus der Wiesche, S., Robertson, M., and Martinez-Botas, R. F. (2020). Experimental facilities for non-ideal compressible vapour flows. In Marek, M., editor, *ERCOFTAC Bulletin nr. 124*, pages 59–66. ERCOFTAC.

Traupel, W. (1952). Zur dynamik realer gase. *Forschung Ing*, 18(1):3–9.

ACKNOWLEDGEMENTS

This research was funded by the Research Council of Finland under Grant number 342135, project *Non-ideal compressible flows in turbomachinery*.